minerals

MDPI

Article

Multi-Proxy Reconstruction of Organic Matter Accumulation and Its Controls in Oligocene–Pliocene Lacustrine Shales, Western Qaidam Basin (China)

Shangkun Li [1,2], Xueyun Ma [1,*], Zhifu Wei [1], Yongli Wang [3], Pengyuan Zhang [4], Gen Wang [1], Kaikang Liang [1,2], Kebin Wei [1,2] and Jianzhen Chen [1,2]

[1] Key Laboratory of Petroleum Resources Exploration and Evaluation, Northwest Institute of Eco-Environment and Resources, Chinese Academy of Sciences, Lanzhou 730000, China; skdsgy@163.com (S.L.)
[2] University of Chinese Academy of Sciences, Beijing 100049, China
[3] Key Laboratory of Cenozoic Geology and Environment, Institute of Geology and Geophysics, Chinese Academy of Sciences, CAS Center for Excellence in Life and Paleoenvironment, Beijing 100029, China
[4] Research Institute of Petroleum Exploration and Development, China National Petroleum Corporation, Beijing 100083, China
* Correspondence: maxueyun@nieer.ac.cn

Abstract

Low-TOC saline lacustrine shales are widespread in Cenozoic basins of northwestern China and Central Asia, yet their organic matter accumulation (OMA) mechanisms under arid, saline conditions remain poorly understood. We analyzed TOC, major and trace elements, and C–O isotopes in 64 core samples from eight wells in the western Qaidam Basin, and reconstructed terrigenous input, weathering intensity, paleoproductivity, redox conditions, and salinity. TOC ranges from 0.04% to 1.10% (mean 0.32%), with a statistically significant upward trend from the Shangganchaigou (mean 0.25%) to the Shangyoushashan Formation (mean 0.43%) (Kruskal–Wallis, p = 0.010). The climate was dry–cold with progressive aridification (increasing $\delta^{18}O$ and Sr/Ba). The water body evolved from closed, strongly reducing, and unstable to more open, weakly reducing, and increasingly saline. We propose that limited nutrient supply set a low baseline for organic enrichment. Weakened terrigenous dilution and enhanced water-column stability then drove the gradual TOC increase. This reveals that OMA can occur without concurrent productivity rise, sustained solely by long-term preservation improvement, offering new constraints for source rock evaluation in arid lacustrine basins.

Keywords: Qaidam Basin; saline lacustrine shale; organic matter accumulation; low-TOC source rock; Paleoenvironmental reconstruction

Check for updates

Academic Editor: Cristina Gama

Received: 10 June 2026
Revised: 10 August 2026
Accepted: 11 August 2026
Published: 14 August 2026

Copyright: © 2026 by the authors. Licensee MDPI, Basel, Switzerland. This article is an open access article distributed under the terms and conditions of the Creative Commons Attribution (CC BY) license.

1. Introduction

In the context of rising global energy demand and declining potential for conventional hydrocarbon resources, unconventional oil and gas have become an important component of the international energy landscape [1]. The degree of organic matter accumulation is a key factor controlling the hydrocarbon generation potential, oil and gas quality, and resource scale of source rocks, and has therefore attracted increasing attention from both academia and industry [2–4]. Previous studies on organic matter accumulation and hydrocarbon potential have largely focused on high-TOC (>2%) sedimentary sequences, such as Devonian black shales in North America, Cretaceous organic-rich deposits in the Tethys Ocean and Atlantic continental shelves, and the Longmaxi Formation in the Sichuan Basin,

China [5–8]. These high-TOC intervals typically formed under the combined influence of high primary productivity and persistent anoxic conditions, resulting in excellent hydrocarbon generation potential. However, such high-TOC deposits are geographically limited and represent only a small proportion of global sedimentary strata.

In contrast, the majority of sedimentary rocks have low TOC contents (<1%). Despite their lower organic richness, these rocks are widely distributed and possess great cumulative thickness, making them globally significant carbon reservoirs with considerable hydrocarbon potential at the regional scale. For example, lacustrine shales in the Shahejie Formation of the Bohai Bay Basin, the Yanchang Formation of the Ordos Basin, and the Xiaganchaigou Formation of the Qaidam Basin commonly exhibit TOC values between 0.2% and 1.5%. Although their organic contents are relatively low, many of these units can still serve as effective source rocks due to sustained reducing conditions [9–11]. Compared with marine systems, organic matter accumulation in lacustrine environments—particularly in saline and closed lakes—is more complex [12]. Lakes are highly sensitive to climatic fluctuations and tectonic activity. Their organic matter enrichment is controlled by the interplay of multiple factors, including primary productivity, redox conditions, salinity, terrigenous input, and sedimentation rate [9,13].

However, most existing models for organic-rich deposition were developed for high-TOC marine or lacustrine settings and cannot be directly applied to low-TOC saline lake systems. Moreover, many studies have focused on single controlling factors while overlooking the complex interactions among them. As a result, the mechanisms of organic matter accumulation in low-TOC lacustrine source rocks remain poorly understood.

The Qaidam Basin, located on the northeastern margin of the Tibetan Plateau, preserves one of the most complete and continuous Cenozoic sedimentary records in Asia. It therefore provides an ideal natural laboratory for investigating the interplay of paleoclimate, tectonic activity, and organic matter accumulation [14,15]. During the Paleogene and Neogene, the basin developed extensive saline lake systems. The lacustrine shales of the Shangganchaigou to Shangyoushashan formations (middle Oligocene to early Pliocene) in the Nanyishan area of the western Qaidam Basin represent a typical low-TOC succession. Although previous work has recognized the hydrocarbon generation potential of these strata, systematic multi-proxy studies on the temporal and spatial variations in organic matter content, its controlling factors, and their links to regional aridification and tectonic uplift are still lacking.

To address this gap, the present study examines core samples from the Shangganchaigou to Shangyoushashan formations in the Nanyishan area of the western Qaidam Basin. We conducted systematic analyses of total organic carbon (TOC), major and trace elements, and carbon and oxygen isotopes, along with related geochemical proxies. By reconstructing terrigenous detrital input, chemical weathering intensity, paleoproductivity, water-column redox conditions, and salinity, and by integrating these results with regional tectonic and climatic evolution, we aim to characterize the variations in organic matter content during this period and identify the dominant controlling factors. The results are expected to improve our understanding of organic matter accumulation mechanisms in low-TOC lacustrine source rocks and to provide a scientific basis for the evaluation and exploration of shale oil and gas resources in the western Qaidam Basin.

2. Geological Setting

The Qaidam Basin is an intracontinental intermontane basin situated along the northern margin of the Tibetan Plateau (Figure 1). It covers an area of approximately 12.1×10^4 km^2 and is bounded to the west by the Altyn Tagh strike-slip fault, to the north by the South Qilian thrust belt, and to the south by the East Kunlun strike-slip thrust belt [16]. The basin formed during the Cenozoic as a result of the India–Eurasia collision and multiple phases of uplift of the Tibetan Plateau [17].

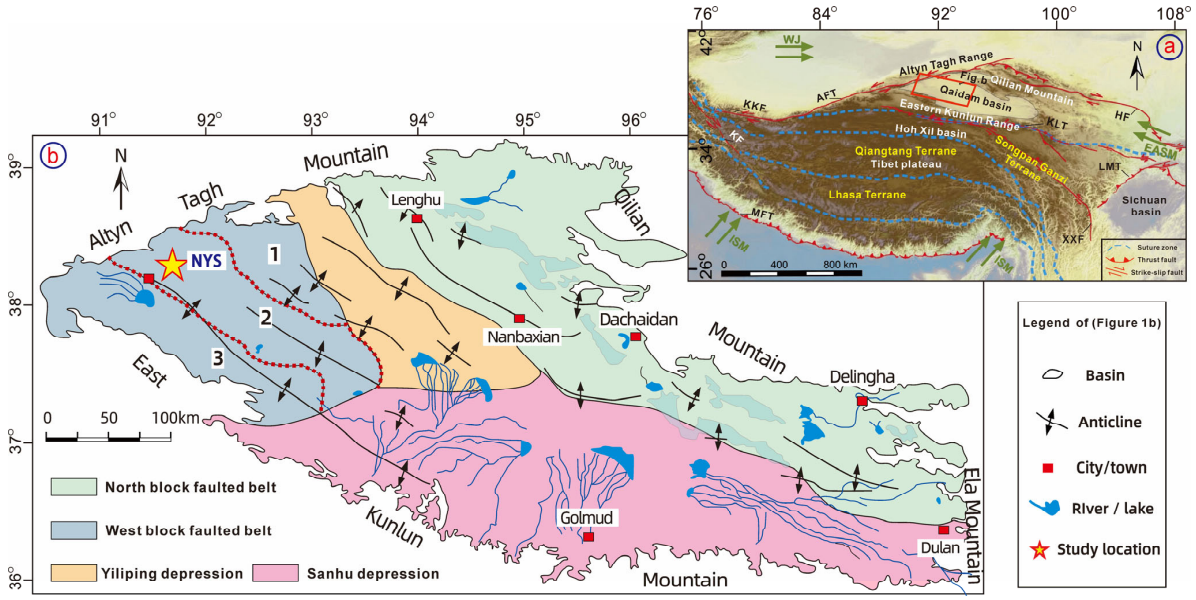


Figure 1. (**a**) DEM map of the Tibetan Plateau and Qaidam Basin (modified from Zhang et al. [18]). MFT: Main frontal thrust, KF: Karakoram fault, KKF: Karakash fault, AFT: Altyn Tagh fault, KLT: Kunlun fault, QNT: Qilian-Nan-Shan thrust belt, XXF: Xianshuihe-Xiaojiang fault system, LMT: Longmen Shan thrust belt, HF: Haiyuan fault. WJ: Westerly Jet, EASM: East Asian Summer Monsoon, ISM: Indian Summer Monsoon. (**b**) Map of the Qaidam Basin showing the surrounding mountains, tectonic sedimentary units, drainage systems, anticlines and study site locations (modified from Zhang et al. [18]). Red dotted lines indicate the boundary of sub-first-level tectonic units: 1—Dafengshan upwarped zone, 2—Mangai depression, and 3—Kunbei faulted terrace zone.

From north to south, the western Qaidam region is divided into four fifth-order structural units: the Yiliping Depression, the Dafengshan Uplift, the Mangya Sag, and the Kunbei Fault Terrace (Figure 1). The basin contains one of the thickest continuous successions of Cenozoic fluvial–lacustrine deposits in the world, reaching approximately 12,000 m in thickness [14]. Based on lithostratigraphy, biostratigraphy, and magnetostratigraphy, previous studies have subdivided the Cenozoic strata of the Qaidam Basin into seven formations [14,19–21]. From bottom to top, these are the Eocene Luhe Formation (E_{1+2}), the Eocene Xiaganchaigou Formation (E_3), the Oligocene–Miocene Shangganchaigou Formation (N_1), the Miocene Xiayoushashan Formation (N_1^2), the Miocene Shangyoushashan Formation (N_2^2), the Miocene–Pliocene Shizigou Formation (N_3^2), and the Lower Pleistocene Qigequan Formation (Q_{1+2}). The sedimentary sequences of these formations record diverse environmental changes that are closely linked to the evolution of organic matter enrichment in saline lacustrine settings.

Three major evolutionary stages are recognized in the western Qaidam basin during the Cenozoic: basin formation and expansion, stable subsidence, and contraction and total closure. The initial stage of basin evolution represents basin opening and expansion, the Altyn Tagh Mountains began to uplift, and the basin subsided gradually, resulting in the deposition of red conglomerates, sandstones, and mudstones of alluvial fan and fluvial facies. From Upper Member of Xiaganchaigou Formation to Shangganchaigou Formation, the basin entered a phase of stable subsidence. Continued uplift of the Altyn Tagh and Kunlun Mountains led to persistent basin deepening and expansion of the water body, during which a succession of gray, organic-rich mudstones and shales was deposited. From Xiayoushashan Formation to Shizigou Formation, the basin evolution is characterized by contraction and extinction. Rapid uplift of the Kunlun Mountains caused the basin to shrink, while the climate became progressively more arid during Shizigou Formation. Evaporation increased markedly, leading to widespread deposition of salt and gypsum, with localized

occurrences of potassium salts such as carnallite [22]. Due to the shallow water depth and high salinity, the Paleogene–Neogene saline source rocks in the western Qaidam region are typically characterized by low organic matter abundance and low thermal maturity.

Consequently, the saline lacustrine source rocks developed in the Paleogene–Neogene strata of the western Qaidam Basin possess distinctive features. These characteristics are jointly controlled by the shallow lacustrine environment and elevated salinity, and are generally expressed as low organic matter content and low thermal maturity. While these features present challenges for research on organic matter accumulation mechanisms in saline lake systems, they also offer valuable opportunities. Clarifying the geological processes responsible for these characteristics is essential for unlocking the hydrocarbon resource potential of the region and for advancing our understanding of organic matter enrichment in saline lacustrine settings.

3. Materials and Methods

Samples were collected from drill cores in the Nanyishan area of the western Qaidam Basin. The cores cover the entire stratigraphic interval from the Shangganchaigou Formation to the Shangyoushashan Formation (Oligocene to Pliocene). The sampling site is located at 38°20′ N, 91°54′ E. The total core thickness is approximately 2450 m and was obtained from eight wells spliced together in stratigraphic order: ZP-1, FX2-3, NQ3-1, NZK01, NQ3-09, NQ22-06, NQ15-023-1, and NQ733 (Figure 2). The dominant lithologies are marl, calcareous mudstone, mudstone, and silty mudstone. A total of 64 samples were selected for analysis, including total organic carbon (TOC) content, major element concentrations by X-ray fluorescence (XRF), trace and rare earth element concentrations by inductively coupled plasma mass spectrometry (ICP-MS), and carbon and oxygen isotope compositions of carbonates. All sample preparation and analytical work was conducted at the Northwest Institute of Eco-Environment and Resources, Chinese Academy of Sciences, and all data are detailed in the Supplementary Materials.

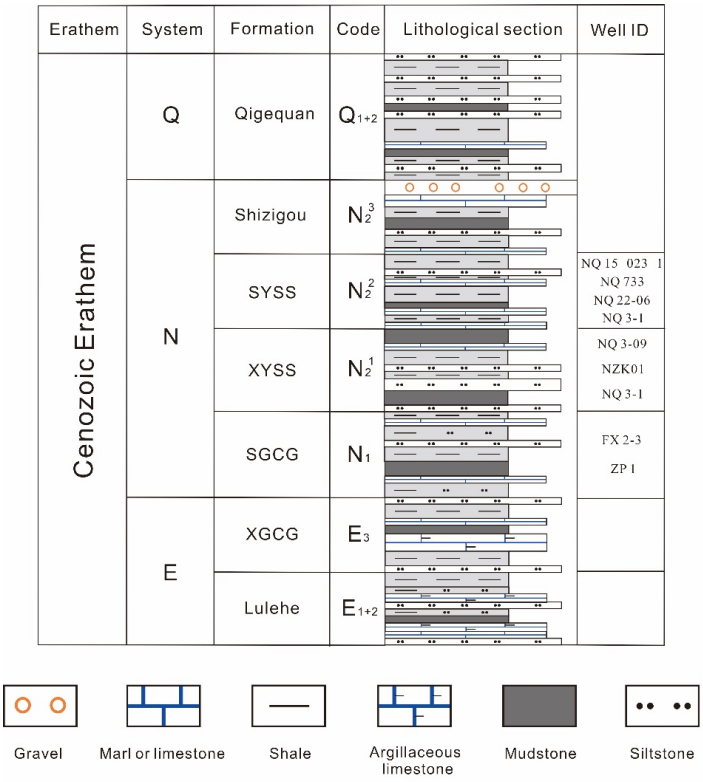


Figure 2. Comprehensive lithostratigraphic column of the Cenozoic in the Western Qaidam area.

3.1. Total Organic Carbon (TOC) Analysis

Prior to TOC analysis, samples were ground to >80 mesh using an agate mortar. Approximately 0.20 g of powdered sample was weighed with a precision of 0.0001 g and placed in a quartz crucible. To remove inorganic carbon, the weighed samples were treated with 6%–7% hydrochloric acid for 24 h. The residues were then rinsed with deionized water until neutral and dried in an oven at 40 °C. The crucibles containing the dried samples were placed on the combustion stage of the instrument. CO_2 generated during combustion was measured by an infrared detector to calculate the TOC content of each sample. Analyses were performed using a LECO CS900 (LECO Corporation, St. Joseph, MI, USA) carbon–sulfur analyzer with a precision of ±5‰.

3.2. X-Ray Fluorescence (XRF) Analysis

Samples were first crushed to >80 mesh using a sample crusher and then further ground to >200 mesh in an agate mortar. Approximately 1 g of powdered sample and 10 g of flux were sequentially added to a crucible and thoroughly mixed with a glass rod. The mixture was transferred to a platinum crucible, and a small amount of LiBr was added as a releasing agent. The platinum crucible was heated at 1200 °C for 20 min. After a series of shaking and homogenization steps, the molten material was poured into a mold and cooled to form a glass disk for analysis. The analytical procedure strictly followed the Chinese national standard GB/T 14506.28-2010 [23]. The analytical uncertainty ranged from 1% to 5%. Major element concentrations were determined using an Axios (PW4400) X-ray (PANalytical, Almelo, The Netherlands)fluorescence spectrometer.

3.3. ICP-MS Analysis of Trace and Rare Earth Elements

All samples were pulverized to <200 mesh for trace element analysis and dried in an oven at 105 °C for 3 h to remove moisture. Approximately 50 mg of powdered sample was placed in a Teflon beaker, and 1.5 mL of high-purity nitric acid was added. After thorough mixing, high-purity hydrofluoric acid and 0.01 mL of perchloric acid (to prevent bumping) were added to decompose silicates. The mixture was evaporated on a hot plate at 140 °C until a wet salt residue remained. The residue was then treated again with 1.5 mL of high-purity nitric acid and hydrofluoric acid, sealed in a steel jacket, and heated in an oven at 195 °C for more than 48 h. After cooling, the solution was evaporated to dryness on a hot plate, followed by the addition of 2 mL of nitric acid and evaporation to a wet salt residue. Subsequently, 3 mL of 50% nitric acid was added, and the beaker was sealed and heated at 150 °C for 24 h. The cooled solution was transferred to a 100 mL PET bottle, and 50 µL of Rh internal standard solution was added. The solution was diluted to 100 g with deionized water so that the final Rh concentration was 10 ng/mL. Trace and rare earth element concentrations were measured using an inductively coupled plasma mass spectrometer (LA-ICP-MS, Nu Attom, Nu Instruments, Wrexham, UK). The analytical uncertainty was less than 3‰, and the procedure followed the Chinese national standard GB/T 14506.30–2010 [24].

3.4. Carbonate Carbon and Oxygen Isotope Analysis

Carbon and oxygen isotope compositions of carbonates were measured using a GasBench system coupled with a Delta V Plus isotope ratio mass spectrometer (Thermo Fisher Scientific, Waltham, MA, USA). Samples were reacted with phosphoric acid at 25 °C for more than 16 h. The generated CO_2 was purified and introduced into the mass spectrometer for isotopic analysis. A laboratory working standard (GBW4416; $\delta^{13}C$ = 1.61‰ VPDB, $\delta^{18}O$ = −11.59‰ VPDB) was analyzed after every eight samples. The analytical precision was better than 0.05‰ for carbon and 0.10‰ (1SD) for oxygen. All measured values were

normalized to the NBS-19 standard at 25 °C ($\delta^{13}C$ = 1.95‰ VPDB, $\delta^{18}O$ = −2.20‰ VPDB). Carbon and oxygen isotope values are reported in per mil (‰) relative to VPDB.

4. Results

4.1. Total Organic Carbon Content

In the Nanyishan area of the western Qaidam Basin, TOC contents in the Shangganchaigou to Shangyoushashan formations range from 0.04% to 1.10%, with a mean value of 0.32%. Formation-specific values are as follows: the Shangganchaigou Formation ranges from 0.04% to 0.99% (mean 0.25%); the Xiayoushashan Formation ranges from 0.07% to 0.83% (mean 0.34%); and the Shangyoushashan Formation ranges from 0.16% to 1.10% (mean 0.43%). Overall, TOC content shows a gradual increase from older to younger strata.

To test whether the differences in TOC content among the three formations are statistically significant, we used the Kruskal–Wallis test (a non-parametric one-way ANOVA). The test statistic H was calculated as:

$$H = [12/N(N+1)] \times \Sigma(R_i^2/n_i) - 3(N+1) \quad (1)$$

where N is the total number of samples, n_i is the sample size of the i-th group, and R_i is the sum of ranks for the i-th group. The resulting H statistic follows a chi-square (χ^2) distribution with df = k − 1 (k = number of groups; here k = 3). The *p*-value was derived from this distribution. The significance level was set at α = 0.05. If the overall test was significant, pairwise comparisons were performed using Dunn's test with Bonferroni correction.

The Kruskal–Wallis test revealed a significant difference in TOC among the Shangganchaigou, Xiayoushashan, and Shangyoushashan formations (H = 9.27, df = 2, p = 0.010). Post hoc pairwise comparisons (Dunn's test with Bonferroni correction) further showed that the Shangyoushashan Formation had significantly higher TOC than the Shangganchaigou Formation (p = 0.016), whereas the Xiayoushashan Formation did not differ significantly from either of the other two formations (p > 0.05), representing a transitional state.

4.2. Elemental Geochemistry and Calculated Proxies

4.2.1. Terrigenous Detrital Input

In the Nanyishan area, Al_2O_3 contents in samples from the Shangganchaigou to Shangyoushashan formations range from 1.47% to 17.16% (mean 11.76%). Mean values for the three formations are similar: 11.71% in the Shangganchaigou Formation, 11.81% in the Xiayoushashan Formation, and 11.87% in the Shangyoushashan Formation. TiO_2 contents range from 0.20% to 0.81% (mean 0.61%), with formation means of 0.63%, 0.60%, and 0.61%, respectively. Zr concentrations vary from 12.82 to 194.46 ppm (mean 128.40 ppm), while Th ranges from 2.87 to 27.54 ppm (mean 14.47 ppm). Ti/Al ratios range from 0.05 to 0.16 (mean 0.06). Overall, the three formations show consistent records of terrigenous detrital input, with only minor fluctuations through time.

4.2.2. Chemical Weathering Intensity

Chemical weathering indices display relatively narrow ranges across the studied interval. CIA values range from 47.30 to 66.21 (mean 62.40), with formation means increasing slightly from 61.61 in the Shangganchaigou Formation to 62.73 in the Xiayoushashan Formation and 63.57 in the Shangyoushashan Formation. CIW values range from 53.45 to 79.65 (mean 75.18), PIA from 46.49 to 74.47 (mean 68.88), and CIX from 59.56 to 72.33 (mean 69.56). All four indices show a weak upward-increasing trend from the Shangganchaigou to the Shangyoushashan Formation, indicating a slight intensification of chemical weathering through time.

4.2.3. Paleoproductivity Proxies

Paleoproductivity indicators exhibit more variable patterns. Si_{bio} contents range widely from 0 to 7,715,656 ppm (mean 18,571.94 ppm), with the highest mean in the Shangganchaigou Formation (23,629.25 ppm) and lower means in the Xiayoushashan (12,736.42 ppm) and Shangyoushashan (15,848.99 ppm) formations. Ba_{bio} ranges from 0 to 2925.24 ppm (mean 244.95 ppm). Nutrient element ratios show the following ranges: Cu/Al from 0.96 to 28.56 (mean 5.74), Ni/Al from 1.02 to 38.15 (mean 6.27), Zn/Al from 1.37 to 96.64 (mean 15.29), and P/Al from 66.76 to 309.94 (mean 98.82). Although most productivity proxies display a slight overall decrease from the Shangganchaigou to the Shangyoushashan Formation, individual indicators show somewhat different temporal patterns.

4.2.4. Redox Conditions

Redox-sensitive proxies indicate relatively stable redox conditions throughout the studied interval. U/Th ratios range from 0.20 to 2.30 (mean 0.47), Ni/Co from 1.14 to 3.11 (mean 2.49), V/Cr from 1.07 to 1.52 (mean 1.30), and V/(V+Ni) from 0.64 to 0.75 (mean 0.71). Enrichment factors show EFU ranging from 1.38 to 24.77 (mean 4.07) and EFMo from 0.15 to 14.35 (mean 4.33). Although some indices exhibit minor fluctuations among the three formations, the overall redox conditions remained relatively stable, with only limited temporal variation.

4.2.5. Salinity

Sr/Ba ratios, used as a salinity proxy, range from 0.19 to 13.44 (mean 1.31). Mean values increase upward through the succession: 1.08 in the Shangganchaigou Formation, 1.31 in the Xiayoushashan Formation, and 1.78 in the Shangyoushashan Formation. This trend indicates a gradual increase in water salinity from older to younger strata.

4.3. Carbonate Carbon and Oxygen Isotope Compositions

Both detrital carbonate input and diagenetic alteration can potentially affect the carbon and oxygen isotope compositions of authigenic carbonates. For example, water–rock interaction involving high-temperature fluids or near-surface fluids during diagenesis can significantly modify the original oxygen isotope values of carbonates [25,26]. Previous studies on different sections in the Qaidam Basin have shown that the contribution of detrital carbonate is generally very limited [27–29]. For instance, Zhuang et al. [28] estimated that detrital carbonate accounts for only about 0.6% of the total carbonate in the Huaitoutala section. Similarly, Guo found that the microscopic characteristics of calcite grains in the Dahonggou section closely resemble those of authigenic carbonates in modern lakes of arid to semi-arid northern China [29], indicating that calcite in the Dahonggou sediments is predominantly authigenic.

The Nanyishan area is dominated by lacustrine deposits, and the core samples were recovered from the depositional center of the basin. In such settings, riverine detrital material tends to settle rapidly near the lake margins due to reduced hydrodynamic energy, particularly in areas with relatively low runoff [30,31]. Therefore, the influence of detrital carbonate input on the Nanyishan core samples is considered to be minimal.

The carbonate oxygen isotope ($\delta^{18}O$) values in this study range from −11.7‰ to −4.08‰, with a mean of −6.19‰. Formation means increase upward: −7.41‰ in the Shangganchaigou Formation, −5.36‰ in the Xiayoushashan Formation, and −4.80‰ in the Shangyoushashan Formation. Carbon isotope ($\delta^{13}C$) values range from −3.48‰ to −0.44‰, with a mean of −1.19‰. The formation means are −1.36‰, −0.82‰, and −1.30‰, respectively. No significant correlation was observed between $\delta^{13}C$ and $\delta^{18}O$

values (R^2 = 0.17; Figure 3), and the isotope compositions fluctuate irregularly with depth. Collectively, these observations indicate that diagenetic alteration has not significantly affected the carbonate isotope compositions. Therefore, the carbon and oxygen isotope data can be reliably used to reconstruct changes in climate and evaporation in the study area.

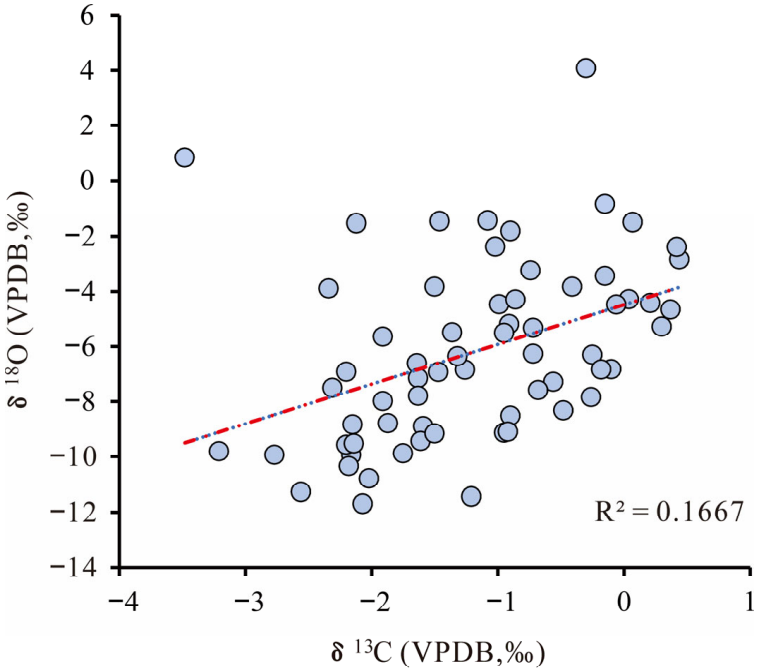


Figure 3. Cross-plot of carbon and oxygen isotope correlation of carbonates from the Shangganchaigou Formation to the Shangyoushashan Formation.The dashed line indicates the linear regression between carbon and oxygen isotopes (R^2 = 0.1667), showing no significant correlation.

5. Discussion

5.1. Paleoclimate and Paleoenvironmental Reconstruction

5.1.1. Terrigenous Detrital Input and Paleoclimate

Terrigenous detrital input influences organic matter enrichment in two principal ways: (1) by regulating the rate of organic matter deposition and burial, and (2) by altering the relative proportion of organic matter within the sediment. Specifically, moderate terrigenous input can supply nutrients that enhance primary productivity and thereby promote organic matter accumulation. However, excessive input may dilute the organic matter content through increased sedimentation of inorganic material, leading to lower organic richness [32–34]. Therefore, reconstructing the history of terrigenous detrital input during shale deposition is essential for identifying the dominant controls on organic matter enrichment.

Elements that are relatively immobile during weathering and diagenesis, such as aluminum (Al), titanium (Ti), zirconium (Zr), and thorium (Th), are widely regarded as reliable proxies for terrigenous detrital input [35–37]. Al and Ti are primarily derived from aluminosilicates and clay minerals transported by rivers into sedimentary basins [37,38]. The Ti/Al ratio is commonly used as an auxiliary indicator of terrigenous input intensity and can effectively reflect changes in sediment provenance or transport conditions [39,40]. In contrast, Zr and Th are concentrated in heavy minerals; thus, Zr/Al ratios can serve as indicators of coarse-grained detrital components [41,42].

In this study, terrigenous detrital input remained relatively stable from the Shangganchaigou to the Shangyoushashan Formation. A slight decrease was observed in the upper part of the Shangganchaigou Formation, followed by a return to average levels. Notably,

although most proxies show consistent overall trends, Th and Zr exhibit somewhat different patterns in the Xiayoushashan Formation. While TiO_2 and Al_2O_3 contents show a slight decrease through this interval, Th and Zr concentrations increase. This discrepancy suggests that the increase in terrigenous input during this period was dominated by heavy minerals, which elevated Zr and Th contents while reducing the relative proportion of TiO_2 (Figure 4).

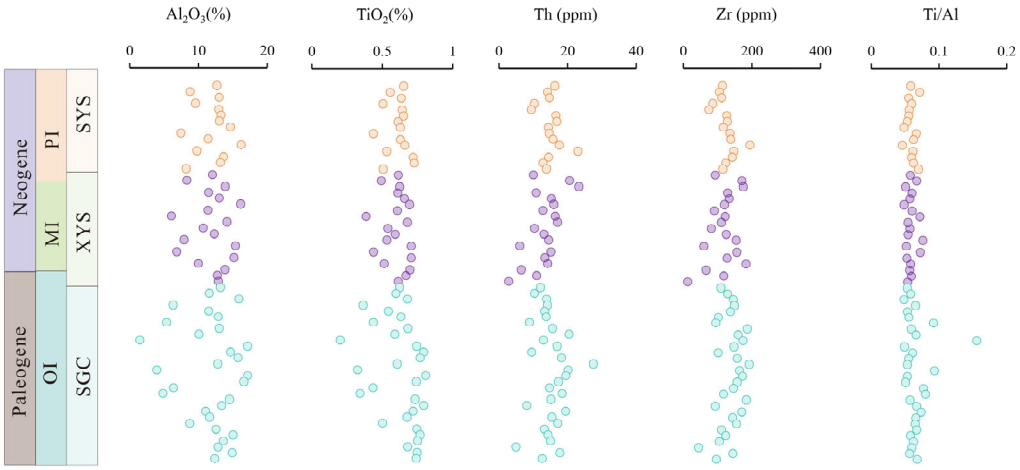


Figure 4. Terrigenous input proxies from the Shangganchaigou to Shangyoushashan formations. Blue: Shangganchaigou Formation; purple: Xiayoushashan Formation; orange: Shangyoushashan Formation.

Terrigenous detrital input is generally controlled by the intensity of continental weathering, which in turn is influenced by tectonic activity (physical weathering) and paleoclimate (chemical weathering). The upper continental crust consists of approximately 21% quartz, 41% plagioclase, and 21% K-feldspar, with feldspar being the most abundant unstable mineral. Chemical weathering of the upper crust is therefore dominated by the breakdown of feldspar and the formation of clay minerals. Calcium (Ca), sodium (Na), and potassium (K) are typically leached from feldspar by aggressive soil solutions, resulting in an increase in the Al_2O_3-to-alkali ratio in the weathering products [43].

Based on this principle, Nesbitt and Young [44] proposed the Chemical Index of Alteration (CIA) as a quantitative measure of weathering intensity. However, Harnois [45] noted that potassium may be leached or retained in residues during weathering, which limits the applicability of CIA in leached sediments. To address this issue, Harnois [45] introduced the Chemical Index of Weathering (CIW), which excludes K_2O. Furthermore, K-metasomatism is common in sedimentary rocks, where K-feldspar replaces plagioclase and can distort weathering indices. Fedo et al. [46] therefore proposed the Plagioclase Index of Alteration (PIA), which further excludes K_2O. More recently, Garzanti et al. [47] developed the CIX index, which excludes CaO to minimize the influence of carbonate minerals. This index offers improved stability in settings with complex provenance.

The calculation formulas for CIA, CIW, PIA, and CIX are provided in Table 1.

Table 1. Summary of weathering intensity indicators.

Indicator Name	Expression	Correlation with Weathering Intensity	References
CIA	$[Al_2O_3/(Al_2O_3 + CaO^* + Na_2O + K_2O)] \times 100$	positive correlation	[44]
CIW	$[Al_2O_3/(Al_2O_3 + CaO^* + Na_2O)] \times 100$		[45]
PIA	$[(Al_2O_3 - K_2O)/(Al_2O_3 - K_2O + CaO^* + Na_2O)] \times 100$		[46]
CIX	$[Al_2O_3/(Al_2O_3 + Na_2O + K_2O)] \times 100$		[47]

For the calculation and correction of CaO*, the following formula is generally applied: $CaO^* = n(CaO) - (10/3) \times n(P_2O_5) - r \times n(CO_2)$. where n denotes molar content. The coefficient r is set to 1 when the carbonate mineral is calcite and to 0.5 when it is dolomite. Because it is often difficult to determine whether the measured CO_2 originates from calcite or dolomite, the correction method proposed by McLennan is commonly adopted: if $n(CaO) < n(Na_2O)$ n, then $n(CaO)$ is used as CaO* for that sample; otherwise, $n(Na_2O)$ is used [48].

The CIA, CIW, and PIA values exhibit similar trends and thus provide consistent information on weathering intensity. Overall, chemical weathering intensity weakened from the lower to the middle part of the Shangyoushashan Formation, followed by alternating fluctuations in the middle to upper parts while remaining at relatively average levels. As shown in Figure 5, CIA is used to quantitatively evaluate the degree of chemical weathering of feldspar. It represents the ratio of Al_2O_3 to unstable oxides and reflects the extent to which feldspar has been converted to clay minerals. Higher CIA values generally indicate greater leaching of K, Na, and Ca from the parent rock and therefore stronger chemical weathering of feldspar [44]. Conventionally, CIA values of 50–70, 70–85, and 85–100 are interpreted to reflect low, moderate, and high degrees of chemical weathering under cold and arid, warm and humid, and warm and wet climatic conditions, respectively [44].

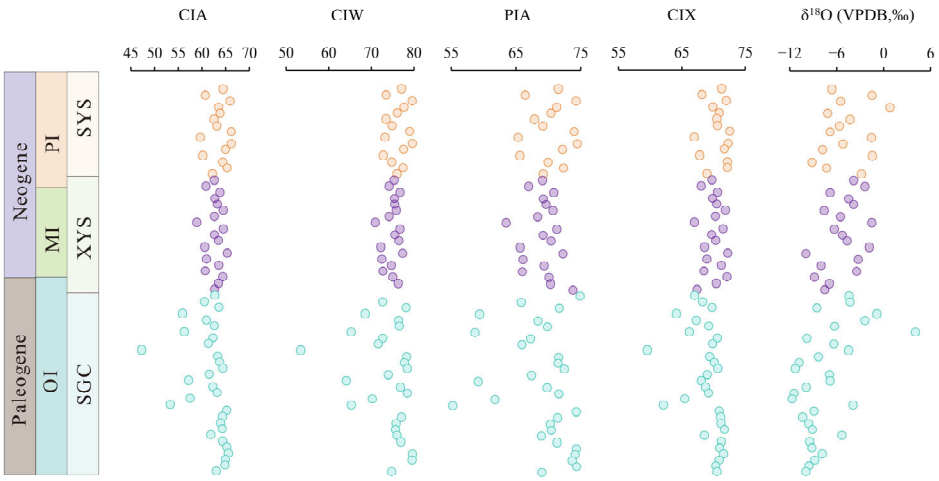


Figure 5. Weathering intensity proxies and carbonate oxygen isotope proxies from the Shangganchaigou Formation to the Shangyoushashan Formation.

Carbonate carbon and oxygen isotope compositions provide additional constraints on the paleoclimatic evolution of the study area. In this study, the mean $\delta^{18}O$ values increase from −7.41‰ in the Shangganchaigou Formation to −4.80‰ in the Shangyoushashan Formation, showing a clear positive shift. In contrast, $\delta^{13}C$ values fluctuate within a narrow range (mean −1.19‰). In a closed lacustrine system, positive shifts in $\delta^{18}O$ are typically interpreted as evidence of enhanced evaporation, as ^{16}O is preferentially removed from the lake water. This interpretation is consistent with the observed increase in Sr/Ba ratios (from 1.08 to 1.78), which indicates rising salinity. Together, these proxies suggest that the degree of regional aridification increased progressively from the Shangganchaigou to the Shangyoushashan Formation. The weathering indices (CIA, CIW, PIA, and CIX) are overall low (mean CIA = 62.40) and show only a slight increase from the Shangganchaigou to the Shangyoushashan Formation. This pattern indicates that the regional climate was generally dry–cold, with limited chemical weathering, consistent with reduced effective precipitation and restricted weathering processes under an aridification regime [44]. Therefore, integrating the carbon and oxygen isotope data, salinity proxies, and weathering indices, we conclude that the climate in the study area from the middle Oligocene to the early

Pliocene (Shangganchaigou to Shangyoushashan formations) was dominated by dry–cold conditions, with a gradual trend toward increasing aridity.

5.1.2. Provenance

Building on the relationships established among terrigenous detrital input, weathering intensity, and paleoclimate, it is necessary to further constrain the provenance of the sediments. Hayashi et al. [38] proposed that the Al_2O_3/TiO_2 ratio of siliciclastic rocks is an effective indicator for discriminating source rock types. In igneous rocks, mafic rocks typically have Al_2O_3/TiO_2 ratios of 3–8, intermediate rocks 8–21, and felsic rocks 21–70. In the present study, Al_2O_3/TiO_2 ratios of the three formations range from 7.26 to 24.56, with a mean of 19.20. Most samples (50 out of 64) yield values below 21, suggesting derivation from intermediate source rocks, although a mixed provenance cannot be ruled out.

Roser and Korsch [49] classified sedimentary provenance into four types based on major element compositions using discriminant function diagrams (F1–F2): (1) mafic igneous provenance (immature oceanic island arc); (2) intermediate igneous provenance (mature magmatic arc or immature continental margin arc); (3) felsic igneous provenance (mature continental margin arc or continental transform margin); and (4) quartzose sedimentary provenance (cratonic interior or recycled orogenic belt, derived from deeply weathered granitic–gneissic or ancient sedimentary sources). In the F1–F2 diagram (Figure 6), most samples from the Shangyoushashan Formation plot within the quartzose sedimentary provenance field, while a few fall into the felsic igneous field. However, detailed examination of the data reveals that the elevated F1 values in some samples are likely caused by high CaO contents resulting from widespread carbonates in the succession. Because the original F1 function assigns a relatively high coefficient (0.616) to CaO, the influence of carbonate minerals leads to overestimation of F1 and distorts the provenance discrimination. This suggests that the sediments were primarily derived from mature continental sources.

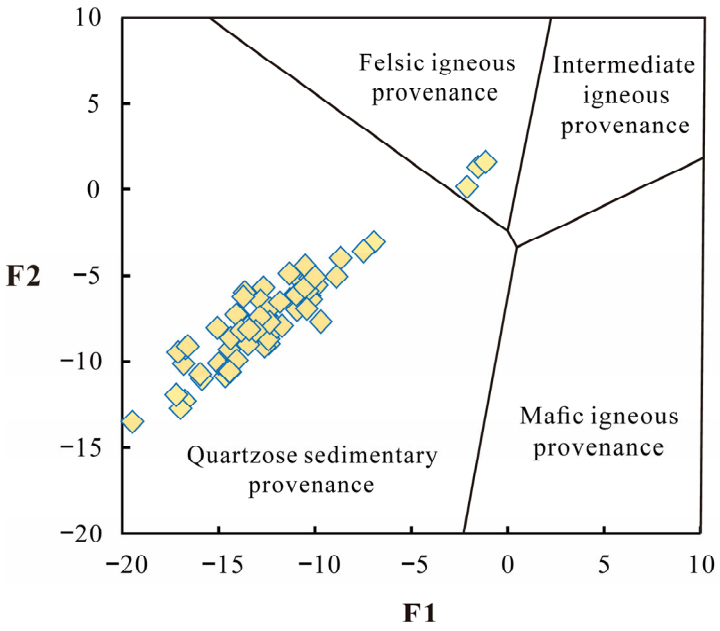


Figure 6. F1–F2 discriminant diagram for provenance discrimination of siliciclastic rocks from the Shangganchaigou to Shangyoushashan formations [49] (pp. 125–130); Squares represent sample points from the Shangganchaigou to Shangyoushashan formations..

Trace element discrimination diagrams provide additional constraints. The La/Yb–∑REE double logarithmic plot [50] shows that most samples cluster near the boundary between sedimentary rocks, granite, and alkaline basalt, indicating a mixed provenance.

The La–Th–Sc ternary diagram [51] suggests that the sediments were mainly derived from a continental island arc setting (Figure 7).

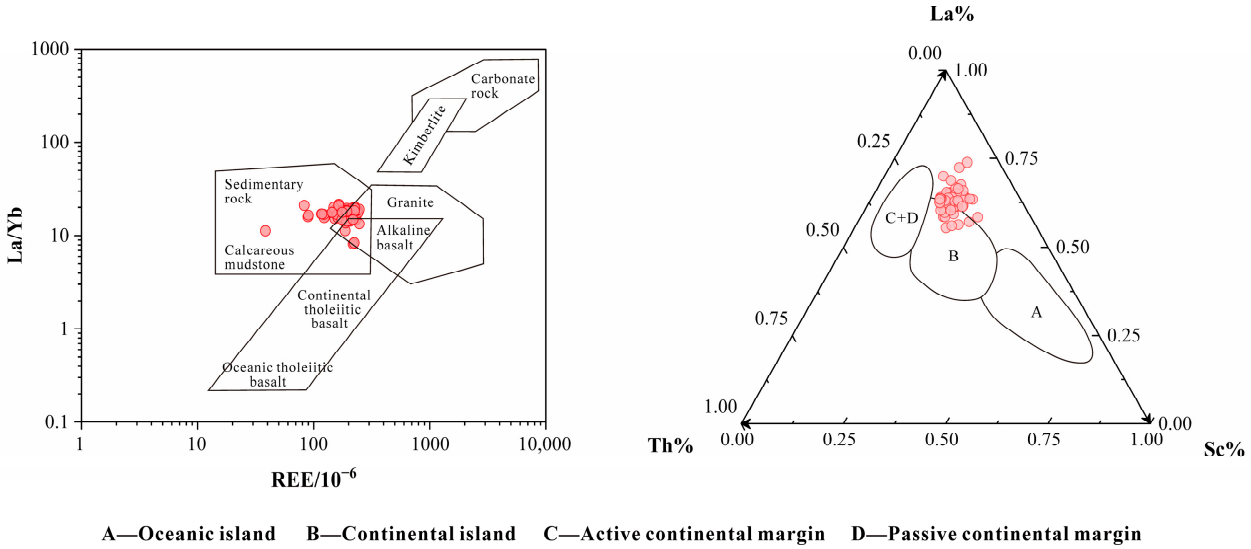


Figure 7. Trace element discrimination diagrams for provenance and tectonic setting of siliciclastic rocks from the western Qaidam Basin. The left panel shows the La/Yb versus ΣREE plot [50] (pp. 4968–4970); the right panel shows the La–Th–Sc ternary diagram [51] (p. 188).

The mountain ranges surrounding the western Qaidam Basin include the southwestern Altyn Tagh and the East Kunlun–Qimantagh Mountains. Higher Al_2O_3/TiO_2 ratios generally reflect contributions from intermediate to felsic igneous rocks such as andesite and granodiorite. The Qimantagh region is widely underlain by Indosinian granodiorite and quartz monzonite, consistent with an intermediate rock signature [52]. In contrast, the southern Altyn Tagh is dominated by metamorphic rocks (gneiss and schist) with limited intermediate igneous lithologies. The F1–F2 diagram indicates a quartzose provenance, pointing to a stable craton or recycled orogenic belt. The Qimantagh region contains Paleozoic carbonates (Ordovician Tanjianshan Group) and Triassic granite, which, upon weathering and transport, can produce quartz-rich detritus. In comparison, the southern Altyn Tagh is characterized by proximal steep fan-delta systems with low textural and compositional maturity (Q/F < 1), inconsistent with a quartzose source. Continental island arc sources are typically dominated by intermediate to felsic volcanic rocks and granodiorite. The Indosinian magmatic activity (ca. 228 Ma) in the Qimantagh region produced granodiorite and porphyry [53], consistent with the continental island arc signature indicated by the La–Th–Sc diagram. The southern Altyn Tagh, however, consists mainly of Precambrian metamorphic basement and lacks evidence of island arc magmatism. The La/Yb–∑REE plot suggests a mixed source, in which sedimentary rocks may represent recycled Ordovician carbonates (e.g., Tanjianshan Group) and Paleozoic clastic rocks, while Indosinian granite in the Qimantagh region may have contributed high ∑REE and fractionated La/Yb ratios. Minor contributions from alkaline basalt may reflect limited extension-related magmatism along the northern margin of the Kunlun Mountains [54].

In summary, the provenance of sediments in the Shangyoushashan Formation of the western Qaidam Basin was dominated by the Qimantagh region (a magmatic belt in the East Kunlun Orogenic Belt characterized by Indosinian granodiorite and Paleozoic carbonates). Indosinian granodiorite and recycled Paleozoic strata jointly controlled the sedimentary characteristics, while the southern Altyn Tagh served only as a minor source. This interpretation is consistent with the regional tectonic evolution (Indosinian subduction–collision) and the depositional system (distal braided delta) [55,56].

5.1.3. Water-Column Redox Conditions, Salinity, and Degree of Restriction

Certain authigenic elements are sensitive to dissolved oxygen levels in the water column and remain relatively immobile after deposition in marine or lacustrine sediments. These elements are therefore widely used as redox-sensitive proxies [37,57–59]. Redox-sensitive elements are generally more soluble under oxic conditions and tend to be removed from the water column, whereas they become enriched in sediments under reducing conditions through authigenic precipitation or adsorption [37].

Although several redox proxies based on redox-sensitive elements (e.g., U/Th, V/Cr, Ni/Co, and V/(V + Ni)) have been applied to reconstruct redox conditions in various geological periods, these proxies frequently yield inconsistent or even contradictory results. Such discrepancies suggest that some redox-sensitive elements are not universally reliable for paleoredox reconstruction across all geological times [60]. Similar inconsistencies were observed in the present study (Figure 8). For example, although vanadium can be enriched in sediments under anoxic conditions, it may precipitate as stable sulfides in the presence of hydrogen sulfide [61]. Nickel and cobalt are not only influenced by redox conditions but are also closely related to paleoproductivity [37], which can obscure the true redox signal. In addition, these trace elements can also be supplied by terrigenous detrital input [35,56,59], meaning that variations in Th content may affect the reliability of redox proxies.

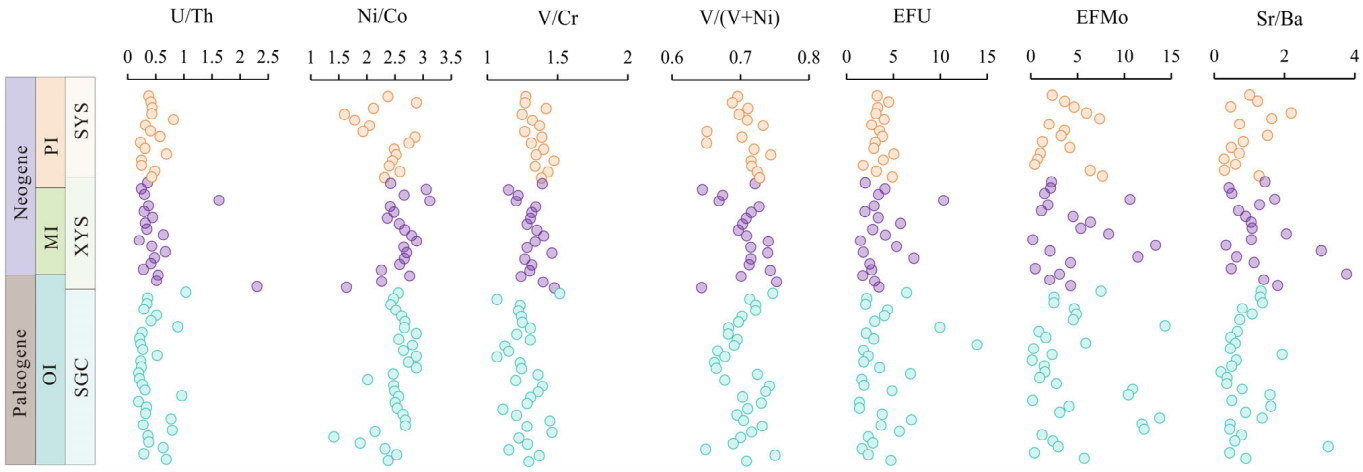


Figure 8. Redox proxies and salinity proxies from the Shangganchaigou Formation to the Shangyoushashan Formation.

In contrast, molybdenum and uranium have low concentrations in the upper continental crust and in planktonic organisms [37] but are commonly enriched in marine and lacustrine sediments under reducing conditions due to authigenic processes [57]. Consequently, Mo and U, particularly when normalized as enrichment factors (EFs), are among the most robust and widely used redox proxies across geological time [37,60,62]. In this study, aluminum was used as the normalizing element to correct for the influence of terrigenous detrital input, following the approach of Van der Weijden [63] and Tribovillard et al. [37]. The enrichment factor is calculated using the following formula [37]:

$$EF_X = (X/Al_{sample})/(X/Al_{criterion\ shale}) \quad (2)$$

where X represents the element of interest, and PAAS denotes the Post-Archean Australian Shale standard composition [35]. Values of EF > 1 indicate enrichment relative to the standard shale, while EF < 1 indicates depletion [37].

EFU and EFMo scatter plots reveal clear stratigraphic trends (Figure 8). In the Shangganchaigou Formation, both EFU and EFMo values are generally high and exhibit con-

siderable variability, with some samples showing notably elevated values. From the Xiayoushashan Formation onward, the values display a gradual decline, which continues into the Shangyoushashan Formation where they decrease further and stabilize. This stratigraphic pattern reflects the evolution of bottom-water redox conditions in the study area. The high and fluctuating EF values in the Shangganchaigou Formation indicate that bottom waters were predominantly suboxic to anoxic, with relatively strong but unstable reducing conditions. This instability may have been related to frequent lake-level fluctuations or periodic disruption of water-column stratification. The progressive decrease and eventual stabilization of EFU and EFMo from the Xiayoushashan to the Shangyoushashan Formation suggest a gradual weakening of bottom-water reducing intensity and a shift toward more stable lake conditions.

The EFMo–EFU covariation plot provides further insight into the degree of water-mass restriction (Figure 9). Samples from the Shangganchaigou Formation show a relatively wide distribution, with several points plotting closer to the anoxic field. In contrast, samples from the Xiayoushashan and Shangyoushashan formations cluster at lower EF values and lie near or below the 1×SW line. This pattern indicates a progressive decrease in the degree of water-mass restriction. The broader distribution and stronger anoxic affinity of Shangganchaigou samples suggest that water exchange was more restricted and fluctuated during this period. The shift of younger samples toward lower EF values and closer to the 1 × SW line reflects a gradual weakening of restricted water circulation and increasing openness of the lake system. According to the Mo–U covariation model proposed by Algeo and Tribovillard [57], the overall offset of data points from the 1×SW line toward lower Mo/U ratios indicates relative depletion of Mo compared to U. This geochemical signature is consistent with restricted water exchange in a closed or semi-closed lake, where Mo is more readily depleted.

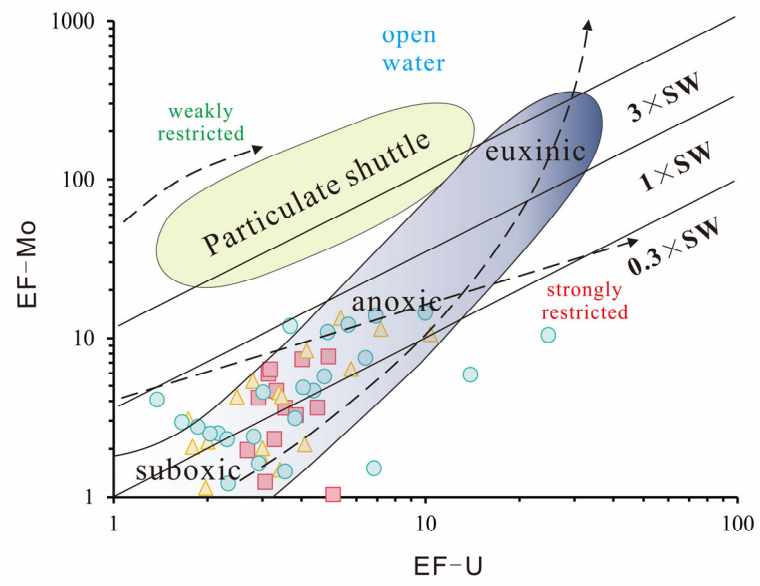


Figure 9. EF-Mo versus EF-U covariation diagram for samples from the Shangganchaigou to Shangyoushashan formations (following Algeo and Tribovillard [58]). Green circles represent sample points from the Shangganchaigou Formation, yellow triangles represent those from the Xiayoushashan Formation, and pink squares represent those from the Shangyoushashan Formation.

Integrating the scatter plots and covariation patterns, the lake water environment in the study area evolved from a relatively restricted, strongly reducing, and unstable state in the Shangganchaigou Formation to a more open, weakly reducing, and stable state in the Shangyoushashan Formation. The scatter plots indicate a progressive weakening

of bottom-water reducing conditions, while the covariation plots further demonstrate a gradual alleviation of water-mass restriction. Together, these trends reflect a transition from strong early restriction and reducing conditions to enhanced water-column mixing and reduced restriction in later times [37].

Water-column stability promotes organic matter enrichment through two main mechanisms. First, it reduces vertical mixing and limits oxygen supply to bottom waters. This helps maintain persistent bottom-water anoxia, even if the reducing conditions are weak. Stable anoxia provides continuous preservation of organic matter. It prevents the intermittent oxidation that happens when stratification breaks down. Second, a stable water column reduces sediment resuspension by wind or currents. This limits the dilution of organic matter by reworked, organic-poor particles.

In our study area, the Shangganchaigou Formation shows high but fluctuating EFU and EFMo values. This indicates strong but unstable reducing conditions. Frequent disruption of stratification likely caused episodic oxygenation and poor preservation. In contrast, the Shangyoushashan Formation has lower and more stable EFU and EFMo values. This reflects weaker but persistent bottom-water anoxia under a more stable water column. Together with reduced terrigenous dilution, this persistent preservation window allowed more organic matter to be preserved, even though productivity remained low. Overall, water-column stability acted as a key control on organic matter enrichment. It sustained stable preservation conditions and suppressed dilution.

Sr/Ba ratios, used as a salinity proxy, show relatively low values in the Shangganchaigou Formation (mean 1.08) (Figure 8). They increase markedly in the early Xiayoushashan Formation, then stabilize at higher levels in the Shangyoushashan Formation (mean 1.78). Although this trend appears contradictory to the weakening of reducing conditions, such a combination is common in closed or semi-closed saline lacustrine systems. In these settings, salinity is primarily controlled by the balance between evaporation and water supply, whereas changes in redox conditions and the degree of restriction mainly reflect variations in deep-water mixing intensity [64,65].

For example, in Cenozoic lacustrine basins around the Tibetan Plateau, regional aridification has intensified evaporation. Even when lake connectivity improves or mixing strengthens, lake water can continue to concentrate, leading to rising salinity [66]. A similar pattern has been documented in other closed lake systems, such as the Eocene Green River Formation in North America, where salinity indicators continued to rise during periods of lake-level fluctuation and enhanced mixing, while bottom-water redox conditions became less reducing due to increased mixing [12,67]. Therefore, even as a lake evolves from a restricted, strongly reducing state toward more open and weakly reducing conditions, salinity can continue to increase if evaporation remains the dominant process. This produces the characteristic combination of decreasing restriction and reducing intensity accompanied by rising salinity [58].

Overall, the lake system in the study area evolved from a relatively closed and strongly reducing state in the Shangganchaigou Formation to a more open and weakly reducing state in the Shangyoushashan Formation. However, salinity continued to rise throughout this interval due to persistent evaporative concentration, reflecting the combined influence of regional aridification and evolving lake hydrology.

5.1.4. Paleoproductivity and Nutrient Sources

Planktonic organisms in lakes provide the primary source of organic matter to the sediment, which can accumulate under favorable depositional conditions [68]. Although numerous proxies have been proposed to reconstruct paleoproductivity, no single indicator is universally reliable [69]. Siliceous organisms, such as radiolarians and certain

planktonic algae, extract dissolved silica from surface waters to build their siliceous skeletons [70]. However, biogenic silica is not the only source of silicon in lacustrine sediments; hydrothermal activity and terrigenous detrital silica are two additional major contributors [71,72]. Hydrothermal fluids typically carry high concentrations of manganese into the water column [73], which can be used to assess whether silica has a hydrothermal origin. The low manganese contents observed in the present samples effectively rule out significant hydrothermal contributions to the silica budget. Therefore, after excluding possible terrigenous silica input, biogenic silica (also referred to as excess silica, Si_{bio}) can serve as a reliable proxy for paleoproductivity [74,75]. Biogenic silica is calculated using the following formula:

$$Si_{bio} = Si_{sample} - Al_{sample} \times (Si/Al)_{PAAS} \quad (3)$$

where Sisample and Alsample represent the silicon and aluminum contents of the sample, respectively, and (Si/Al)PAAS is the ratio in Post-Archean Australian Shale [35].

Heavy barite is the main carrier of barium in lacustrine sediments and forms as a product of plankton decomposition after death [76]. Following the decay of plankton, microbial aggregates settle through the water column, resulting in a close relationship between sedimentary barium concentrations and surface-water productivity [77,78]. Consequently, barium is commonly deposited as biogenic barite and has been widely used as a paleoproductivity proxy [37]. Biogenic barium (Ba_{bio}), calculated by subtracting the terrigenous barium component, is the fraction typically employed in paleoproductivity reconstructions. It is calculated as follows:

$$Ba_{bio} = Ba_{sample} - Al_{sample} \times (Ba/Al)_{PAAS} \quad (4)$$

where Basample and Alsample represent the barium and aluminum contents of the sample, respectively, and (Ba/Al)PAAS is the ratio in Post-Archean Australian Shale [35].

Several nutrient elements, including copper, nickel, and phosphorus, play fundamental roles in lacustrine biogeochemical cycles and are closely linked to primary producers and productivity [37,74,79,80]. Copper is taken up by primary producers during photosynthesis and can be preserved in sediments as sulfides under anoxic conditions [80,81]. Nickel occurs in highly stable tetrapyrrole complexes within chlorophyll and is preserved in sediments as silicates under reducing conditions [77]. Phosphorus is an essential nutrient that controls primary productivity over both short and long timescales and is preserved in sediments as phosphate minerals after organism death [6]. After correcting for terrigenous input, these nutrient-related elements can be applied to reconstruct paleoproductivity [37]. Therefore, Ni/Al, Cu/Al, and P/Al ratios are also used as paleoproductivity proxies.

In this study, Ba_{bio} and Si_{bio} exhibit inconsistent trends from the Shangganchaigou to the Shangyoushashan Formation. Ba_{bio} values are notably low in the Shangganchaigou Formation, rise sharply in the early Xiayoushashan Formation, and then decline significantly again (Figure 10). This pattern is likely influenced by redox conditions rather than reflecting true productivity changes. Authigenic barite is well preserved under oxic conditions but dissolves in the water column under anoxic conditions [82,83]. In the early Shangganchaigou Formation, the progressive shift from oxic to anoxic bottom waters would have increased barite dissolution, while the subsequent return to more oxic conditions in the middle to late Shangganchaigou Formation would have reduced dissolution. Given the overall stronger reducing conditions during this interval, enhanced barite dissolution likely prevented reliable Ba_{bio} enrichment. In fact, Ba_{bio} values are generally low under oxic conditions throughout geological history. Therefore, Ba_{bio} is not considered a reliable productivity indicator in this study, and paleoproductivity is inferred to have remained relatively low throughout the Shangganchaigou to Shangyoushashan interval.

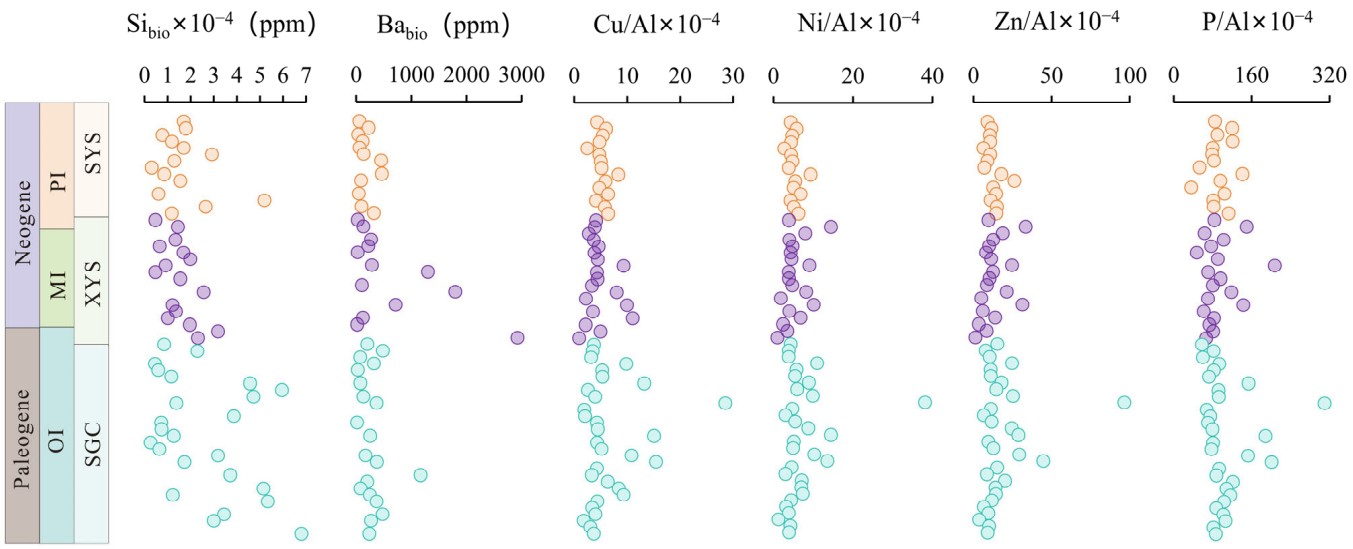


Figure 10. Paleoproductivity proxies from the Shangganchaigou Formation to the Shangyoushashan Formation.

Although Ni/Al, Cu/Al, and P/Al ratios can also reflect paleoproductivity, these elements are themselves influenced by redox conditions (Figure 10). Phosphorus tends to be enriched under anoxic conditions [6], while Cu and Ni are also preferentially preserved under reducing environments [79]. Consequently, their ratios may partly reflect redox variations rather than productivity alone. In this study, Ni/Al, Cu/Al, and P/Al ratios show trends similar to those of Si_{bio}. Given these considerations, Si_{bio} is regarded as the most reliable paleoproductivity proxy in the present dataset.

The maintenance of lacustrine primary productivity depends on a continuous supply of nutrients, among which phosphorus, nitrogen, and silicon are particularly important for phytoplankton growth [74]. In closed or semi-closed lacustrine systems, nutrients are mainly derived from chemical weathering and physical erosion of surrounding mountain ranges, followed by fluvial transport into the lake [6,84]. Provenance analysis indicates that sediments in the western Qaidam Basin were primarily sourced from the Qimantagh region, where Indosinian granodiorite and recycled Paleozoic strata provided a stable supply of terrigenous material. Although terrigenous input remained relatively constant throughout the studied interval (with only a slight decrease in the upper Shangganchaigou Formation), the low chemical weathering intensity (indicated by CIA, CIW, PIA, and CIX values) suggests that nutrient release from bedrock was limited under the prevailing dry–cold climate. Furthermore, the progressive increase in salinity (Sr/Ba rising from 1.08 to 1.78) reflects enhanced evaporation, which likely reduced the bioavailability of dissolved nutrients. Collectively, the low and relatively stable Si_{bio} values, together with the nutrient element ratios (Ni/Al, Cu/Al, and P/Al), indicate that nutrient supply remained at low levels from the Shangganchaigou to the Shangyoushashan Formation. This limited nutrient availability was an important factor constraining organic matter enrichment during this period.

Furthermore, the statistical analysis of TOC values across the three formations shows a statistically significant upward trend from the Oligocene Shangganchaigou Formation to the Pliocene Shangyoushashan Formation (Kruskal–Wallis, $p = 0.010$). This result rules out the possibility that the TOC variation is merely random fluctuation and confirms a systematic increase over time.

It should be noted that statistical significance does not imply a large magnitude of increase. The mean TOC values of the Shangganchaigou and Shangyoushashan formations

are 0.25% and 0.43%, respectively. Although the former is generally lower and the latter relatively higher, both remain within a low TOC range (<0.5%). This indicates that organic matter enrichment was consistently constrained by some background factor and maintained at a low level, despite the gradual increase in TOC. This is consistent with our argument that limited nutrient supply serves as the primary background constraint—nutrient limitation sets an upper limit for organic matter enrichment, so that TOC remains within a low range even with a significant trend.

Under this background constraint, the statistically significant TOC increase can be attributed to the superimposed effects of other factors. Specifically, the progressive weakening of terrigenous detrital dilution and the enhancement of water-column stability allowed a greater proportion of the limited organic matter produced to be preserved. The Xiayoushashan Formation, as a transitional stage, shows no significant difference from either end-member formation, further supporting a gradual process rather than an abrupt event. Overall, nutrient supply determined the low baseline of organic matter enrichment, while dilution intensity and preservation conditions modulated the magnitude and trend of TOC variation above this baseline.

5.2. Organic Matter Accumulation Patterns and Driving Mechanisms

In the Nanyishan area of the western Qaidam Basin, TOC contents in shales from the Shangganchaigou to Shangyoushashan formations are overall low, with a mean value of 0.32%. However, TOC shows a gradual upward increase from the Shangganchaigou Formation (mean 0.25%) to the Shangyoushashan Formation (mean 0.43%). This trend is controlled by the combined effects of terrigenous detrital input intensity, redox conditions, water salinity, and the regional dry–cold to aridification climate. Weathering indices are generally low, indicating weak chemical weathering and limited nutrient supply. Terrigenous detrital input remained relatively stable throughout the studied interval, although the distribution of high-value intervals varies among formations. Carbonate $\delta^{18}O$ values show a progressive positive shift from a mean of $-7.41‰$ in the Shangganchaigou Formation to $-4.80‰$ in the Shangyoushashan Formation, indicating enhanced evaporation and increasing regional aridification. This trend is consistent with the upward increase in Sr/Ba ratios. Within this paleoenvironmental framework, each formation exhibits distinct organic matter characteristics and controlling factors.

The Shangganchaigou Formation has the lowest organic matter content. During this interval, EFU and EFMo values are highest, indicating relatively strong reducing conditions in bottom waters and favorable preservation. However, terrigenous detrital input shows several high-value intervals, resulting in strong dilution effects. In addition, salinity was elevated in some intervals. These factors collectively offset the preservation advantage provided by reducing conditions. Furthermore, low chemical weathering intensity limited nutrient release, maintaining TOC at low levels (Figure 11a).

Organic matter content increased in the Xiayoushashan Formation relative to the Shangganchaigou Formation. Although EFU and EFMo values decreased, indicating weaker reducing conditions and less favorable preservation, terrigenous input became more stable (with fewer high-value intervals), reducing the dilution effect. At the same time, the degree of water-mass restriction decreased and the lake environment became more stable. These changes likely compensated for the weaker preservation conditions, allowing better organic matter accumulation. Although $\delta^{18}O$ values continued to shift positively and salinity increased, the rise had not yet reached levels that strongly suppressed biological production. Therefore, the increase in TOC in this formation was primarily driven by reduced dilution and increasing water-column stability (Figure 11b).

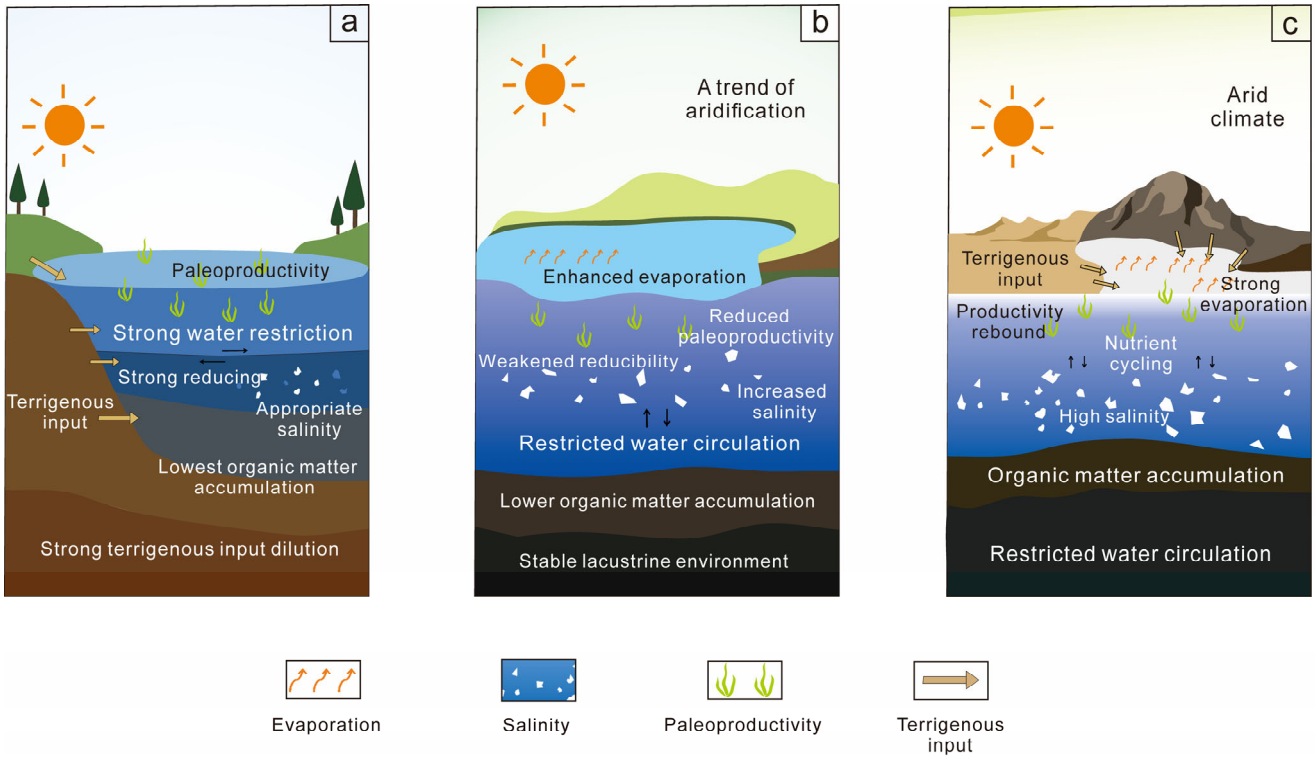


Figure 11. Schematic diagrams of organic matter accumulation models from the Shangganchaigou Formation to the Shangyoushashan Formation: (**a**) organic matter accumulation model of the Shangganchaigou Formation; (**b**) organic matter accumulation model of the Xiayoushashan Formation; (**c**) organic matter accumulation model of the Shangyoushashan Formation.

The Shangyoushashan Formation records the highest organic matter content among the three formations. Although EFU and EFMo values decreased further, indicating the weakest reducing conditions and reduced preservation efficiency, terrigenous input remained stable without significant intensification of dilution. Water-mass restriction reached its lowest level and the lake environment was most stable. Although $\delta^{18}O$ values show the strongest positive shift, the overall hydrological conditions appear to have been more balanced, potentially favoring nutrient recycling. Consequently, despite continued weakening of preservation conditions, TOC reached its highest values in this formation, driven primarily by stable dilution levels, maximum water-column stability, and a slight improvement in productivity (Figure 11c).

Overall, organic matter content in the study area shows a slow upward increase from the Shangganchaigou to the Shangyoushashan Formation, but remains at low levels throughout. The dry–cold regional climate (reflected by low chemical weathering intensity) and tectonically stable terrigenous supply together resulted in limited nutrient availability. The Shangganchaigou Formation was characterized by strong reducing preservation offset by strong dilution. The Xiayoushashan Formation experienced reduced dilution and increasing water stability, leading to higher TOC. The Shangyoushashan Formation achieved the highest TOC under stable dilution and the most stable water conditions. In summary, limited nutrient supply was the primary factor constraining organic matter content, while changes in the degree of terrigenous dilution and water-column stability were the main mechanisms modulating the gradual increase in TOC through time.

6. Conclusions

This study examined core samples from the Shangganchaigou to Shangyoushashan formations (middle Oligocene to early Pliocene) in the Nanyishan area of the western

Qaidam Basin. Through systematic analyses of total organic carbon, major and trace elements, carbon and oxygen isotopes, and related geochemical proxies, we reconstructed terrigenous detrital input, chemical weathering intensity, paleoproductivity, water-column redox conditions, and salinity. We then discussed the patterns and primary controls on organic matter accumulation. The main conclusions are as follows:

(1) The climate in the study area was predominantly dry–cold from the Shangganchaigou to Shangyoushashan formations, with a progressive trend toward aridification, as indicated by the positive shift in $\delta^{18}O$ and the continuous increase in Sr/Ba ratios. The water environment evolved from a relatively closed, strongly reducing state in the early stage to a more open, weakly reducing but increasingly saline state in the later stage. Shale TOC contents are overall low (mean 0.32%) but show a statistically significant upward trend from the Shangganchaigou to the Shangyoushashan Formation.

(2) Organic matter content differs among the three formations. The Shangganchaigou Formation has the lowest TOC, likely because strong reducing conditions favorable for preservation were offset by intense terrigenous dilution (high-value intervals) and locally elevated salinity. TOC increased in the Xiayoushashan Formation, possibly due to more stable terrigenous input (reduced dilution) and increasing water-column stability. The Shangyoushashan Formation records the highest TOC among the three formations, which may reflect stable dilution levels, the most stable water environment, and a slight improvement in productivity indicators.

(3) Limited nutrient supply under the dry–cold regional climate constrained the overall low baseline of organic matter content. Superimposed on this background, the progressive weakening of terrigenous dilution and the enhancement of water-column stability jointly drove the statistically significant, gradual increase in TOC through time. We propose that nutrient supply set the lower limit of organic matter enrichment, while dilution and preservation efficiency modulated the temporal trend. This study reveals a specific enrichment pattern for low-TOC lacustrine shales under arid climate conditions. In this pattern, primary productivity set a low baseline. Weakened dilution and persistently enhanced water-column stability together improved long-term preservation conditions. This allowed organic matter to accumulate gradually, without a concurrent rise in productivity. This finding suggests that favorable source rock intervals may develop in zones with stable water-column stratification and moderate terrigenous input. This can serve as a reference for hydrocarbon exploration in saline lacustrine basins of arid regions. Future studies could combine higher-resolution sampling, organic petrology, and biomarker analysis. This would help clarify the fine-scale mechanisms linking water-column stability and organic matter preservation.

Supplementary Materials: The following supporting information can be downloaded at: https://www.mdpi.com/article/10.3390/min16080839/s1, Table S1: All experimental data.

Author Contributions: Conceptualization, S.L.; methodology, S.L.; formal analysis, S.L.; investigation, S.L.; data curation, S.L.; writing—original draft preparation, S.L.; writing—review and editing, S.L., Y.W., P.Z., G.W., K.L., K.W. and J.C.; supervision, Z.W.; project administration, X.M.; funding acquisition, X.M. All authors have read and agreed to the published version of the manuscript.

Funding: This research was funded by the National Natural Science Foundation of China, grant numbers 42502106, 42472019, 42372223 and 42402165; the Theory of Hydrocarbon Enrichment under Multi-Spheric Interactions of the Earth, grant number THEMSIE04010101; and the National Key R&D Program of China, grant numbers 2022YFF0800800 and 2024YFF0809102. The APC was funded by grant number 42502106.

Data Availability Statement: All data supporting the reported results are provided in the Supplementary Materials (Table S1).

Acknowledgments: We thank the laboratory staff at the Northwest Institute of Eco-Environment and Resources, Chinese Academy of Sciences for their assistance in sample preparation and analysis. The authors are grateful to the academic editor and anonymous reviewers for their constructive comments.

Conflicts of Interest: Pengyuan Zhang is an employee of China National Petroleum Corporation. The paper reflects the views of the scientists and not the company.

References

1. Sun, L.; Liu, H.; Zhu, R.; Cui, B.; Lei, Z.; Meng, S.; Tang, J. Ten Noteworthy Issues on Shale Oil Revolution in China. *Acta Pet. Sin.* **2023**, *44*, 2007–2019. [CrossRef]
2. Kong, X.; Jiang, Z.; Zhang, K.; Zhang, Y. Organic matter enrichment and hydrocarbon accumulation mechanisms in lacustrine shale: A case study of the Triassic Yanchang Formation, Ordos Basin, China. *Mar. Pet. Geol.* **2020**, *116*, 104312. [CrossRef]
3. Liu, H.; Zou, C.; Zhu, R.; Wu, S.; Cui, J.; Qiu, Z.; Liu, G.; Zhang, M. Accumulation Mechanism of Organic Matters in Paleogene Qaidam Basin, Northwestern China. *J. Earth Sci.* **2025**, *36*, 2117–2137. [CrossRef]
4. Sun, J.; Dang, W.; Wang, F.; Nie, H.; Wei, X.; Li, P.; Zhang, S.; Feng, Y.; Li, F. Prediction of TOC content in organic-rich shale using machine learning algorithms: Comparative study of random forest, support vector machine, and XGBoost. *Energies* **2023**, *16*, 4159. [CrossRef]
5. Sageman, B.B.; Murphy, A.E.; Werne, J.P.; Ver Straeten, C.A.; Hollander, D.J.; Lyons, T.W. A tale of shales: The relative roles of production, decomposition, and dilution in the accumulation of organic-rich strata, Middle–Upper Devonian, Appalachian basin. *Chem. Geol.* **2003**, *195*, 229–273. [CrossRef]
6. Algeo, T.J.; Ingall, E. Sedimentary Corg: P ratios, paleocean ventilation, and Phanerozoic atmospheric pO2. *Palaeogeogr. Palaeoclimatol. Palaeoecol.* **2007**, *256*, 130–155. [CrossRef]
7. Jenkyns, H.C. Geochemistry of oceanic anoxic events. *Geochem. Geophys. Geosystems* **2010**, *11*, Q03004. [CrossRef]
8. Zou, C.; Dong, D.; Wang, Y.; Li, X.; Huang, J.; Wang, S.; Guan, Q.; Zhang, C.; Wang, H.; Liu, H.; et al. Shale gas in China: Characteristics, challenges and prospects (I). *Pet. Explor. Dev.* **2015**, *42*, 753–767. [CrossRef]
9. Zhang, P.; Jiang, F.; Zhu, C.; Huang, R.; Hu, T.; Xu, T.; Li, W.; Xiong, H. Gas generation potential and characteristics of oil-prone shale in the saline lacustrine rifting basins: A case study of the Dongpu Depression, Bohai Bay Basin. *Energy Fuels* **2021**, *35*, 2192–2208. [CrossRef]
10. Zou, C.; Yang, Z.; Cui, J.; Hou, L.; Dong, D.; Wang, Y.; Wang, S. Formation mechanism, geological characteristics and development strategy of nonmarine shale oil in China. *Pet. Explor. Dev.* **2013**, *40*, 14–26. [CrossRef]
11. Li, G.; Jin, Z.; Li, X.; Zhang, P.; Liang, X.; Zhang, R.; Li, C.; Wang, D.; Hu, Y. Shallow burial shale gas accumulation pattern of the Wufeng–Longmaxi Formations in the northern Guizhou area, western Yangtze platform. *Geoenergy Sci. Eng.* **2023**, *225*, 211683. [CrossRef]
12. Bohacs, K.M.; Carroll, A.R.; Neal, J.E.; Mankiewicz, P.J. Lake-basin type, source potential, and hydrocarbon character: An integrated sequence-stratigraphic-geochemical framework. In *Lake Basins Through Space and Time*; Gierlowski-Kordesch, E.H., Kelts, K.R., Eds.; AAPG Studies in Geology 46; AAPG: Tulsa, OK, USA, 2000; pp. 3–34.
13. Ning, Y.; Liu, H.; Zavala, C.; Chen, H.; Shi, W.; Lan, X.; Zhou, L. The impact of extensional and strike-slip composite tectonic activity on the development of fine-grained sedimentary rocks and the enrichment of organic matter in lacustrine rift basin: Insights from the Paleogene of the Shanan Sag, Bohai Offshore Basin. *Mar. Pet. Geol.* **2025**, *182*, 107574. [CrossRef]
14. Fang, X.; Zhang, W.; Meng, Q.; Gao, J.; Wang, X.; King, J.; Song, C.; Dai, S.; Miao, Y. High-resolution magnetostratigraphy of the Neogene Huaitoutala section in the eastern Qaidam Basin on the NE Tibetan Plateau, Qinghai Province, China and its implication on tectonic uplift of the NE Tibetan Plateau. *Earth Planet. Sci. Lett.* **2007**, *258*, 293–306. [CrossRef]
15. Song, C.; Hu, S.; Han, W.; Zhang, T.; Fang, X.; Gao, J.; Wu, F. Middle Miocene to earliest Pliocene sedimentological and geochemical records of climate change in the western Qaidam Basin on the NE Tibetan Plateau. *Palaeogeogr. Palaeoclimatol. Palaeoecol.* **2014**, *395*, 67–76. [CrossRef]
16. Yuan, J.Y.; Chen, Q.L.; Chen, Y.B.; Yan, C.F. Petroleum geological character and favorable exploration domains of Qaidam Basin. *Nat. Gas. Geosci.* **2006**, *17*, 640–644. (In Chinese)
17. Xiong, Y.; Tan, X.; Wu, K.; Xu, Q.; Liu, Y.; Qiao, Y. Petrogenesis of the Eocene lacustrine evaporites in the western Qaidam Basin: Implications for regional tectonic and climate changes. *Sediment. Geol.* **2021**, *416*, 105867. [CrossRef]
18. Zhang, T.; Han, W.; Fang, X.; Miao, Y.; Zhang, W.; Song, C.; Wang, Y.; Khatri, D.B.; Zhang, Z. Tectonic control of a change in sedimentary environment at ~10 Ma in the northeastern Tibetan Plateau. *Geophys. Res. Lett.* **2018**, *45*, 6843–6852. [CrossRef]

19. Song, B.; Zhang, K.; Lu, J.; Wang, C.; Xu, Y. The middle Eocene to early Miocene integrated sedimentary record in the Qaidam Basin and its implications for paleoclimate and early Tibetan Plateau uplift. *Can. J. Earth Sci.* **2013**, *50*, 183–196. [CrossRef]
20. Fang, X.; Galy, A.; Yang, Y.; Zhang, W.; Ye, C.; Song, C. Paleogene global cooling–induced temperature feedback on chemical weathering, as recorded in the northern Tibetan Plateau. *Geology* **2019**, *47*, 992–996. [CrossRef]
21. Ji, J.; Zhang, K.; Clift, P.D.; Zhuang, G.; Song, B.; Ke, X.; Xu, Y. High-resolution magnetostratigraphic study of the Paleogene-Neogene strata in the Northern Qaidam Basin: Implications for the growth of the Northeastern Tibetan Plateau. *Gondwana Res.* **2017**, *46*, 141–155. [CrossRef]
22. Chen, Y.; Xia, X.M.; Li, Y.N.; Zhao, J.; Cui, J.; Qiao, B.H.; Zhao, D.S.; Gao, H.C.; Wang, Y.; Tan, L.; et al. Lacustrine sedimentary characteristics of the Pliocene Xiayoushashan Formation in Xianshuiquan area, Western Qaidam Basin: A case study from cored interval of Well Xiandong 1. *Acta Sedimentol. Sin.* **2023**, *42*, 619–631. [CrossRef]
23. *GB/T 14506.28-2010*; Methods for Chemical Analysis of Silicate Rocks—Part 28: Determination of 16 Major and Minor Components. Standards Press of China: Beijing, China, 2010.
24. *GB/T 14506.30-2010*; Methods for Chemical Analysis of Silicate Rocks—Part 30: Determination of 44 Elements. Standards Press of China: Beijing, China, 2010.
25. Garzione, C.N.; Dettman, D.L.; Horton, B.K. Carbonate oxygen isotope paleoaltimetry: Evaluating the effect of diagenesis on paleoelevation estimates for the Tibetan Plateau. *Palaeogeogr. Palaeoclimatol. Palaeoecol.* **2004**, *212*, 119–140. [CrossRef]
26. Leier, A.L.; Quade, J.; DeCelles, P.G.; Kapp, P. Stable isotopic results from paleosol carbonate in South Asia: Implications for Miocene environmental change. *Earth Planet. Sci. Lett.* **2009**, *279*, 204–214. [CrossRef]
27. Kent-Corson, M.L.; Ritts, B.D.; Zhuang, G.; Bovet, P.M.; Graham, S.A.; Chamberlain, C.P. Stable isotope constraints on the tectonic, topographic, and climatic evolution of the northern margin of the Tibetan Plateau. *Earth Planet. Sci. Lett.* **2009**, *282*, 158–166. [CrossRef]
28. Zhuang, G.; Brandon, M.T.; Pagani, M.; Krishnan, S. Isotopic constraints on intensified aridity in Central Asia around 12 Ma. *Earth Planet. Sci. Lett.* **2011**, *312*, 152–163. [CrossRef]
29. Guo, L. Aridification Processes and Mechanisms at Different Timescales: A Case Study of the Qaidam Basin and Sandy Lands in Northern China. Ph.D. Thesis, Institute of Geology and Geophysics, Chinese Academy of Sciences, Beijing, China, 2019. (In Chinese)
30. Deckker, P.D.; Corrège, T.; Head, J. Late Pleistocene record of cyclic eolian activity from tropical Australia suggesting the Younger Dryas is not an unusual climatic event. *Geology* **1991**, *19*, 602–605. [CrossRef]
31. Long, H.; Lai, Z.P.; Wang, N.L.; Li, Y. Holocene climate variations from Zhuyeze terminal lake records in East Asian monsoon margin in arid northern China. *Quat. Res.* **2010**, *74*, 46–56. [CrossRef]
32. Dypvik, H.; Harris, N.B. Geochemical facies analysis of fine-grained siliciclastics using Th/U, Zr/Rb and (Zr+Rb)/Sr ratios. *Chem. Geol.* **2001**, *181*, 131–146. [CrossRef]
33. Calvert, S.E.; Pedersen, T.F. Chapter fourteen—Elemental proxies for palaeoclimatic and palaeoceanographic variability in marine sediments: Interpretation and application. *Dev. Mar. Geol.* **2007**, *1*, 567–644. [CrossRef]
34. März, C.; Schnetger, B.; Brumsack, H.J. Nutrient leakage from the North Pacific to the Bering Sea (IODP Site U1341) following the onset of Northern Hemispheric Glaciation? *Paleoceanography* **2013**, *28*, 68–78. [CrossRef]
35. Taylor, S.R.; McLennan, S.M. *The Continental Crust: Its Composition and Evolution*; Blackwell: Oxford, UK, 1985.
36. Zhang, T.; Kershaw, S.; Wan, Y.; Lan, G. Geochemical and facies evidence for palaeoenvironmental change during the Late Ordovician Hirnantian glaciation in South Sichuan Province, China. *Glob. Planet. Change* **2000**, *24*, 133–152. [CrossRef]
37. Tribovillard, N.; Algeo, T.J.; Lyons, T.; Riboulleau, A. Trace metals as paleoredox and paleoproductivity proxies: An update. *Chem. Geol.* **2006**, *232*, 12–32. [CrossRef]
38. Hayashi, K.I.; Fujisawa, H.; Holland, H.D.; Ohmoto, H. Geochemistry of ~1.9 Ga sedimentary rocks from northeastern Labrador, Canada. *Geochim. Cosmochim. Acta* **1997**, *61*, 4115–4137. [CrossRef] [PubMed]
39. Chen, H.F.; Yeh, P.Y.; Song, S.R.; Hsu, S.C.; Yang, T.N.; Wang, Y.; Chi, Z.Q.; Lee, T.Q.; Chen, M.T.; Cheng, C.L.; et al. The Ti/Al molar ratio as a new proxy for tracing sediment transportation processes and its application in aeolian events and sea level change in East Asia. *J. Asian Earth Sci.* **2013**, *73*, 31–38. [CrossRef]
40. Jiménez-Espejo, F.J.; Yeh, P.Y.; Song, S.R.; Hsu, S.C.; Yang, T.N.; Wang, Y.; Chi, Z.; Lee, T.Q.; Chen, M.T.; Cheng, C.L.; et al. Detrital input, productivity fluctuations, and water mass circulation in the westernmost Mediterranean Sea since the Last Glacial Maximum. *Geochem. Geophys. Geosyst.* **2008**, *9*, Q11003. [CrossRef]
41. Young, G.M.; Nesbitt, H.W. Processes controlling the distribution of Ti and Al in weathering profiles, siliciclastic sediments and sedimentary rocks. *J. Sediment. Res.* **1998**, *68*, 448–455. [CrossRef]
42. Hofmann, P.; Wagner, T. ITCZ controls on Late Cretaceous black shale sedimentation in the tropical Atlantic Ocean. *Paleoceanography* **2011**, *26*, PA4223. [CrossRef]
43. Wedepohl, K. Untersuchungen am Kupferschiefer in Nordwestdeutschland; Ein Beitrag zur Deutung der Genese bituminöser Sedimente. *Geochim. Cosmochim. Acta* **1964**, *28*, 305–364. [CrossRef]

44. Nesbitt, H.W.; Young, G.M. Early Proterozoic climates and plate motions inferred from major element chemistry of lutites. *Nature* **1982**, *299*, 715–717. [CrossRef]
45. Harnois, L. The CIW index: A new chemical index of weathering. *Sediment. Geol.* **1988**, *55*, 319–322. [CrossRef]
46. Fedo, C.M.; Nesbitt, H.W.; Young, G.M. Unraveling the effects of K metasomatism in sedimentary rocks and paleosols with implications for palaeoweathering conditions and provenance. *Geology* **1995**, *23*, 921–924.
47. Garzanti, E.; Vermeesch, P.; Padoan, M.; Resentini, A.; Vezzoli, G.; Andò, S. Provenance of passive-margin sand (Southern Africa). *J. Geol.* **2014**, *122*, 17–42. [CrossRef] [PubMed]
48. McLennan, S.M.; Hemming, S.; McDaniel, D.K.; Hanson, G.N. Geochemical approaches to sedimentation, provenance, and tectonics. *Geol. Soc. Am. Spec. Pap.* **1993**, *284*, 101–104. [CrossRef]
49. Roser, B.P.; Korsch, R.J. Provenance signatures of sandstone-mudstone suites determined using discriminant function analysis of major-element data. *Chem. Geol.* **1988**, *67*, 119–139. [CrossRef]
50. Cullers, R.L. The controls on the major and trace element variation of shales, siltstones, and sandstones of Pennsylvanian–Permian age from uplifted continental blocks in Colorado to platform sediment in Kansas, USA. *Geochim. Cosmochim. Acta* **1994**, *58*, 4955–4972. [CrossRef]
51. Bhatia, M.R.; Crook, K.A.W. Trace element characteristics of graywackes and tectonic setting discrimination of sedimentary basins. *Contrib. Mineral. Petrol.* **1986**, *92*, 181–193. [CrossRef]
52. Shen, X.; Jian, X.; Zhang, W.; Ye, S.; Liang, H.; Zhuang, Y.; Guan, P. Provenance of Cenozoic sandstones in the Qaidam Basin and implications for tectonic evolution of the northern Tibetan Plateau. *Palaeogeogr. Palaeoclimatol. Palaeoecol.* **2025**, *675*, 113120. [CrossRef]
53. Feng, C.Y.; Wang, S.; Li, G.C.; Ma, S.C.; Li, D.S. Middle to Late Triassic granitoids in the Qimantage area, Qinghai Province, China: Chronology, geochemistry and metallogenic significances. *Acta Petrol. Sin.* **2012**, *28*, 665–678.
54. Jian, X.; Weislogel, A.; Pullen, A.; Shang, F. Formation and evolution of the Eastern Kunlun Range, northern Tibet: Evidence from detrital zircon U-Pb geochronology and Hf isotopes. *Gondwana Res.* **2020**, *83*, 63–79. [CrossRef]
55. Dong, Y.; He, D.; Sun, S.; Liu, X.; Zhou, X.; Zhang, F.; Yang, Z.; Cheng, B.; Zhao, G.; Li, J. Subduction and accretionary tectonics of the East Kunlun orogen, western segment of the Central China Orogenic System. *Earth-Sci. Rev.* **2018**, *186*, 231–261. [CrossRef]
56. Qin, G.S.; Wu, S.H.; Song, X.M.; Zou, C.Y.; Zheng, L.Y.; Chen, C. Sedimentary characteristics and single sand body architecture analysis of distal fine-grained braided river delta. *J. China Univ. Pet. (Ed. Nat. Sci.)* **2017**, *41*, 9–19. [CrossRef]
57. Algeo, T.J.; Maynard, J.B. Trace-element behavior and redox facies in core shales of Upper Pennsylvanian Kansas-type cyclothems. *Chem. Geol.* **2004**, *206*, 289–318. [CrossRef]
58. Algeo, T.J.; Tribovillard, N. Environmental analysis of paleoceanographic systems based on molybdenum–uranium covariation. *Chem. Geol.* **2009**, *268*, 211–225. [CrossRef]
59. Algeo, T.J.; Rowe, H. Paleoceanographic applications of trace-metal concentration data. *Chem. Geol.* **2012**, *324–325*, 6–18. [CrossRef]
60. Algeo, T.J.; Li, C. Redox classification and calibration of redox thresholds in sedimentary systems. *Geochim. Cosmochim. Acta* **2020**, *287*, 8–26. [CrossRef]
61. Brumsack, H.J. Geochemistry of recent TOC-rich sediments from the Gulf of California and the Black Sea. *Geol. Rundsch.* **1989**, *78*, 851–882. [CrossRef]
62. Tribovillard, N.; Algeo, T.J.; Baudin, F.; Riboulleau, A. Analysis of marine environmental conditions based on molybdenum–uranium covariation—Applications to Mesozoic paleoceanography. *Chem. Geol.* **2012**, *324–325*, 46–58. [CrossRef]
63. Van der Weijden, H.C. Pitfalls of normalization of marine geochemical data using a common divisor. *Mar. Geol.* **2002**, *184*, 167–187. [CrossRef]
64. Eugster, H.P.; Hardie, L.A. Saline lakes. In *Lakes: Chemistry, Geology, Physics*; Lerman, A., Ed.; Springer: New York, NY, USA, 1978; pp. 237–293.
65. Carroll, A.R.; Bohacs, K.M. Stratigraphic classification of ancient lakes: Balancing tectonic and climatic controls. *Geology* **1999**, *27*, 99–102. [CrossRef]
66. Ye, C.; Yang, Y.; Fang, X.; Zhang, W.; Song, C.; Yang, R. Paleolake Salinity Evolution in the Qaidam Basin (NE Tibetan Plateau) between ~42 and 29 Ma: Links to Global Cooling and Paratethys Sea Incursions. *Sediment. Geol.* **2020**, *409*, 105778. [CrossRef]
67. Surdam, R.C.; Stanley, K.O. Lacustrine sedimentation during the culminating phase of Eocene Lake Gosiute, Wyoming (Green River Formation). *Geol. Soc. Am. Bull.* **1979**, *90*, 93–110. [CrossRef]
68. Macquaker, J.H.S.; Keller, M.A.; Davies, S.J. Algal blooms and "marine snow": Mechanisms that enhance preservation of organic carbon in ancient fine-grained sediments. *J. Sediment. Res.* **2010**, *80*, 934–942. [CrossRef]
69. Averyt, K.B.; Paytan, A. A comparison of multiple proxies for export production in the equatorial Pacific. *Paleoceanography* **2004**, *19*, PA4003. [CrossRef]
70. Lyle, M.; Murray, D.W.; Finney, B.P.; Dymond, J.; Robbins, J.M.; Brooksforce, K. The record of late Pleistocene biogenic sedimentation in the eastern tropical Pacific Ocean. *Paleoceanography* **1988**, *3*, 39–59. [CrossRef]

71. Grützner, J.; Hillenbrand, C.D.; Rebesco, M. Terrigenous flux and biogenic silica deposition at the Antarctic continental rise during the late Miocene to early Pliocene: Implications for ice sheet stability and sea ice coverage. *Glob. Planet. Change* **2005**, *45*, 131–149. [CrossRef]
72. Fan, H.; Wen, H.; Zhu, X.; Hu, R.; Tian, S. Hydrothermal activity during Ediacaran–Cambrian transition: Silicon isotopic evidence. *Precambrian Res.* **2013**, *224*, 23–35. [CrossRef]
73. Cowen, J.P.; Massoth, G.J.; Baker, E.T. Bacterial scavenging of Mn and Fe in a mid- to far-field hydrothermal particle plume. *Nature* **1986**, *322*, 169–171. [CrossRef]
74. Algeo, T.J.; Kuwahara, K.; Sano, H.; Bates, S.; Lyons, T.; Elswick, E.; Hinnov, L.; Ellwood, B.; Moser, J.; Maynard, J.B. Spatial variation in sediment fluxes, redox conditions, and productivity in the Permian–Triassic Panthalassic Ocean. *Palaeogeogr. Palaeoclimatol. Palaeoecol.* **2011**, *308*, 65–83. [CrossRef]
75. Shen, J.; Algeo, T.J.; Hu, Q.; Xu, G.; Zhou, L.; Feng, Q. Volcanism in South China during the Late Permian and its relationship to marine ecosystem and environmental changes. *Glob. Planet. Change* **2013**, *105*, 121–134. [CrossRef]
76. Griffith, E.M.; Paytan, A. Barite in the ocean—Occurrence, geochemistry and palaeoceanographic applications. *Sedimentology* **2012**, *59*, 1817–1835. [CrossRef]
77. Ganeshram, R.S.; Pedersen, T.F.; Calvert, S.E.; McNeill, G.W.; Fontugne, M.R. Glacial–interglacial variability in denitrification in the world's oceans: Causes and consequences. *Paleoceanography* **2000**, *15*, 361–376. [CrossRef]
78. Jeandel, C.; Tachikawa, K.; Bory, A.; Dehairs, F. Biogenic barium in suspended and trapped material as a tracer of export production in the tropical NE Atlantic (EUMELI sites). *Mar. Chem.* **2000**, *71*, 125–142. [CrossRef]
79. Lewan, M.D.; Maynard, J.B. Factors controlling enrichment of vanadium and nickel in the bitumen of organic sedimentary rocks. *Geochim. Cosmochim. Acta* **1982**, *46*, 2547–2560. [CrossRef]
80. Piper, D.Z.; Perkins, R.B. A modern vs. Permian black shale—The hydrography, primary productivity, and water-column chemistry of deposition. *Chem. Geol.* **2004**, *206*, 177–197. [CrossRef]
81. Algeo, T.J.; Lyons, T.W. Mo–total organic carbon covariation in modern anoxic marine environments: Implications for analysis of paleoredox and paleohydrographic conditions. *Paleoceanography* **2006**, *21*, PA1016. [CrossRef]
82. Bishop, J.K.B. The barite–opal–organic carbon association in oceanic particulate matter. *Nature* **1988**, *332*, 341–343. [CrossRef]
83. Dehairs, F.; Stroobants, N.; Goeyens, L. Suspended barite as a tracer of biological activity in the Southern Ocean. *Mar. Chem.* **1991**, *35*, 399–410. [CrossRef]
84. Meyers, S.R. Production and preservation of organic matter: The significance of iron. *Paleoceanography* **1997**, *12*, 563–578. [CrossRef]

Disclaimer/Publisher's Note: The statements, opinions and data contained in all publications are solely those of the individual author(s) and contributor(s) and not of MDPI and/or the editor(s). MDPI and/or the editor(s) disclaim responsibility for any injury to people or property resulting from any ideas, methods, instructions or products referred to in the content.